clean technologies

MDPI

Article

A Numerical Investigation of the Potential of an Enhanced Geothermal System (EGS) for Power Generation at Mount Meager, BC, Canada

Yutong Chai [1], Zhuoheng Chen [2], Wanju Yuan [2] and Shunde Yin [1,*]

[1] Department of Civil and Environmental Engineering, University of Waterloo, Waterloo, ON N2L 3G1, Canada; y5chai@uwaterloo.ca
[2] Geological Survey of Canada, Natural Resources Canada, Calgary, AB T2L 2A7, Canada; zhuoheng.chen@nrcan-rncan.gc.ca (Z.C.); wanju.yuan@nrcan-rncan.gc.ca (W.Y.)
* Correspondence: shunde.yin@uwaterloo.ca; Tel.: +519-888-4567 (ext. 33323)

Abstract: This study aims to better harness the geothermal potential of Mount Meager in British Columbia, a premier reserve of geothermal resources in Canada. Numerical investigations explore the feasibility and optimization of an Enhanced Geothermal System to boost geothermal energy extraction capabilities. Utilizing COMSOL Multiphysics, the model simulates non-isothermal fluid flow and heat transfer through complex subsurface geology with discrete fracture planes. The sensitivity analyses assess the impact of various operational parameters, including injection strategies, reservoir characteristics, and wellbore configurations on heat extraction efficiency. These analyses indicate that a higher injection rate, lower injection temperatures, and optimized fracture areas significantly enhance system performance by maximizing thermal energy capture and minimizing thermal breakthrough. Additionally, specific wellbore configurations, particularly the triplet setup with deeper depth, significantly improve geothermal fluid circulation and heat extraction compared to doublet configurations at shallower depths. This study reveals that the base case scenario of the EGS could generate approximately 8.311×10^9 kWh over 30 years, while optimization strategies could elevate potential production to up to 16.68×10^9 kWh. These findings underscore the critical role of carefully designed operational strategies that leverage local geological and thermal characteristics to optimize geothermal systems, thereby enhancing efficiency and promoting sustainable energy development at Mount Meager.

Keywords: geothermal energy; enhanced geothermal system (EGS); heat extraction performance

check for updates

Academic Editor: Alessandro Cannavale

Received: 21 October 2024
Revised: 23 January 2025
Accepted: 5 February 2025
Published: 7 February 2025

Citation: Chai, Y.; Chen, Z.; Yuan, W.; Yin, S. A Numerical Investigation of the Potential of an Enhanced Geothermal System (EGS) for Power Generation at Mount Meager, BC, Canada. *Clean Technol.* **2025**, *7*, 14. https://doi.org/10.3390/cleantechnol7010014

Copyright: © 2025 by the authors. Licensee MDPI, Basel, Switzerland. This article is an open access article distributed under the terms and conditions of the Creative Commons Attribution (CC BY) license (https://creativecommons.org/licenses/by/4.0/).

1. Introduction

Under the increasing demand to achieve carbon neutrality, the development of renewable energy sources like geothermal energy production is critical. Geothermal provides a sustainable and low-carbon alternative to conventional fossil fuels, drastically reducing greenhouse gas emissions [1]. Geothermal energy is exceptionally versatile, capable of delivering both electricity and direct-use thermal energy, making it an essential player in the decarbonization of multiple sectors. In colder regions such as British Columbia, where energy needs are substantial and solar power is less, geothermal energy assumes a critical role in fostering zero-energy communities. By integrating geothermal systems into community-scale initiatives, regions can generate both electric and thermal energies that predominantly support local consumption, reducing the need for extensive energy imports and exports [2].

Mount Meager, located in British Columbia, Canada, is an ideal site for the development of geothermal energy due to its unique geological and geothermal characteristics. As a potentially active volcanic site, Mount Meager's subsurface is naturally heat-enriched [3]. Previous exploration has identified a geothermal reservoir at a shallow depth of less than 1 km, with an aerial extent of 4.5 to 7.5 km^2 and an average temperature ranging from 220 °C to 240 °C, with a maximum receorded temperature of 275 °C [4,5]. Flow testing conducted in the mid-2000s demonstrated hydraulic connectivity between existing wells over a zone at least 730 m in length. This suggests that the volcanic rocks at reservoir depth are likely naturally fractured, providing pathways that could be further enhanced through hydraulic fracturing to increase permeability and fracture connectivity. These favourable conditions for geothermal development may be attributed to either underground fluid being heated at great depths or volcanic activity in the region [6]. Additionally, the site's remote location minimizes the potential for environmental impact on populated areas, while its proximity to surface facilities could facilitate the integration of geothermal energy into the existing power grid, enhancing the overall stability and sustainability of the energy system [1]. These factors, combined with the ongoing research and previous studies conducted by our team have confirmed the potential of geothermal exploitation, make Mount Meager a prime candidate for various geothermal development initiatives.

Enhanced Geothermal System (EGS) has emerged as a transformative approach in renewable energy, extracting geothermal power from areas previously considered unsuitable due to the absence of conventional hydrothermal resources [7,8]. This innovative technology involves artificially creating or enhancing fracture connections in deep hot dry rock (HDR) formations, allowing for the extraction of heat from the Earth's core. The history of EGS dates back to the late 1970s, initiated by the pioneering work at Fenton Hill, New Mexico, conducted by the Los Alamos National Laboratory [9]. This project demonstrated the potential of EGS in regions devoid of natural hydrothermal activity and laid the groundwork for future exploration and exploitation of geothermal energy worldwide. In today's context, EGS stands as a critical component in the global shift towards sustainable energy solutions, capable of providing substantial baseload power while contributing significantly to economic stability and reducing reliance on fossil fuels and other non-sustainable resources [10,11].

The advancement of EGS is closely tied to the evolution of numerical simulation techniques, which have become increasingly sophisticated with the growth of computational power. Early models were simplistic but set the stage for the development of more complex simulation tools capable of capturing the intricate interactions within the subsurface [12,13]. The more recent numerical models are often supported by robust software platforms such as COMSOL, Fluent, and CMG STARS. COMSOL has self-defining partial different equations and strong coupling of multiple physical problems, operating under the Finite Element Method (FEM) [14]. The FEM is highly advantageous for dealing with complex geometries and heterogeneous material properties typical of geothermal reservoirs. It provides high accuracy in spatial discretization and can efficiently handle irregular boundaries and anisotropic media. However, the FEM can be computationally intensive and requires sophisticated meshing techniques, which may increase the complexity of the model setup [15]. Hu et al. [16] presented a COMSOL model to investigate the feasibility of utilizing geothermal energy from EGS as a heat source for oil sands separation by using discrete fractures, demonstrating the potential of saving natural gas and reducing greenhouse gas emissions from the thermal production. Fluent by ANSYS is a Finite Volume Method (FVM)-based software. The FVM is particularly strong in conservation properties, making it suitable for modelling fluid flow and heat transfer in geothermal applications. It offers a simpler approach to discretization compared to the FEM and is easier

to implement on structured grids. Nonetheless, the FVM might struggle with geometric complexity and may require more effort to achieve high accuracy in regions with steep gradients [17]. Luo et al. [18] performed the modeling of EGS with CO_2 instead of water as the working fluid due to the additional benefit of CO_2 geological storage during the power generation. A numerical model built with Fluent is constructed and sensitivity analyses are conducted, focusing on the influence of injection rate, permeability of induced fractures, well perforation placement, and the heat transfer between wellbores and the reservoir. The Computer Modelling Group (CMG) is a reservoir numerical simulation software inclined to production practice using the Finite Difference Method (FDM), with STARS as its thermal and advanced processes simulator. FDM is the simplest and most direct approach, ideal for quick preliminary assessments and educational purposes. It is easy to implement but is generally less flexible in handling complex boundary conditions and non-uniform grid distributions, potentially limiting its use in accurately modelling more intricate geothermal systems [19]. Zeinali et al. [20] presented a solution to find the most cost-effective well and fracture spacing to supply hot fluid to the power generation plant by proposing a three-well pattern that employs a multiple transverse fractured horizontal well drilled and fractured in hot dry rocks. The numerical studies are conducted using STARS to model the circulation of cold water injected into the centre of a radial transverse hydraulic fracture and produced from two horizontal wells. Different commercial software is characterized by their distinct pros and cons; therefore, the final decision of which software to be used to simulate for EGS is still up to researchers to choose based on their individual needs and focuses.

Researchers employing these numerical tools have explored various parameters and configurations to optimize the performance and sustainability of EGSs. The configuration of injection and extraction wells, for instance, is a critical factor that influences the efficiency of heat extraction. Studies have investigated configurations ranging from single-well setups to complex multi-well arrangements, assessing their impact on the overall energy recovery and economic viability of EGS projects [21–23]. In addition, various well placements—ranging from simple vertical configurations [16] to horizontal wells [24,25], inclined designs [26], and multilateral wells [27]—have been explored with innovation in mind by both industry and academia. Furthermore, numerical simulations are routinely used to optimize operational parameters such as injection pressure and temperature, fluid type and behavior, and flow rate, aiming to maximize thermal output while minimizing negative impacts like induced seismicity, which remains a significant concern associated with EGSs [28,29]. Additionally, the geological characteristics of EGS sites, including rock type and existing natural fractures, significantly influence the design and expected performance of EGSs, as these factors affect how artificially created fractures propagate and how effectively injected fluids can transport heat. Since most feasibility analyses are conducted before the precise characterization of local geological parameters and rock properties, researchers have employed probabilistic studies and sensitivity analyses to quantify these uncertainties [13,30].

Recognizing the vast geothermal heat reserves at Mount Meager and the technical advancements in EGS, we conducted numerical studies to assess the potential for implementing EGS at Mount Meager and to optimize its energy extraction efficiency. In this paper, we present a thermal-hydro coupled model built with the COMSOL Multiphysics. This study will serve as a feasibility study for the implementation of EGS application at Mount Meager, examined a vertical well pair under base case parameters and conduct sensitivity analyses under various operation conditions, reservoir characteristics, and wellbore configurations.

2. Methodology

2.1. Geology and Fracture Characterization at Mount Meager

The Meager Mountain Volcanic Complex (MMVC) is a high-temperature geothermal system with an identified geothermal reservoir of fractured quartz diorite in the basement [4]. Although efforts have been made to produce the heat energy resource, insufficient flow from the production tests prevented commercial development using conventional methods. A better understanding of the existing natural fracture networks and how they can impact the in-situ stress state which controls the geometry of the induced fracture networks at depth which is considered as the reservoir for EGS development can be crucial.

In 2019, the Geological Survey of Canada performed a field study in Mount Meager, examining fractures in the intrusive and metamorphic basement rocks as well as the overlying volcanic rocks. Figure 1 provides a summary map of the orientation and dip of major fracture groups based on these field observations and existing geological interpretations [31]. Preliminary analysis identifies at least three distinct types of fractures, each associated with different geological processes. Fractures from regional tectonic deformation, consistent in character, are common in the basement rocks, often aligning spatially with volcanic eruption centres/vents and seismic activity. These tectonic lineaments typically strike NW-SE, aligning with the major horizontal compressional stress orientations. Fractures linked to volcanic doming and eruptive activities show geographical variability, forming circular or radial segments with strikes changing relative to the eruption centres, as observed in interpreted Landsat fault/fracture zones [32]. These volcanic activities can complicate and reactivate pre-existing tectonic fractures. Additionally, gravitational fractures, prevalent in volcanic terrains and aligned parallel to slopes, contribute to instability in mountain ridges and peaks, potentially triggering events like the 2010 Mount Meager landslide.

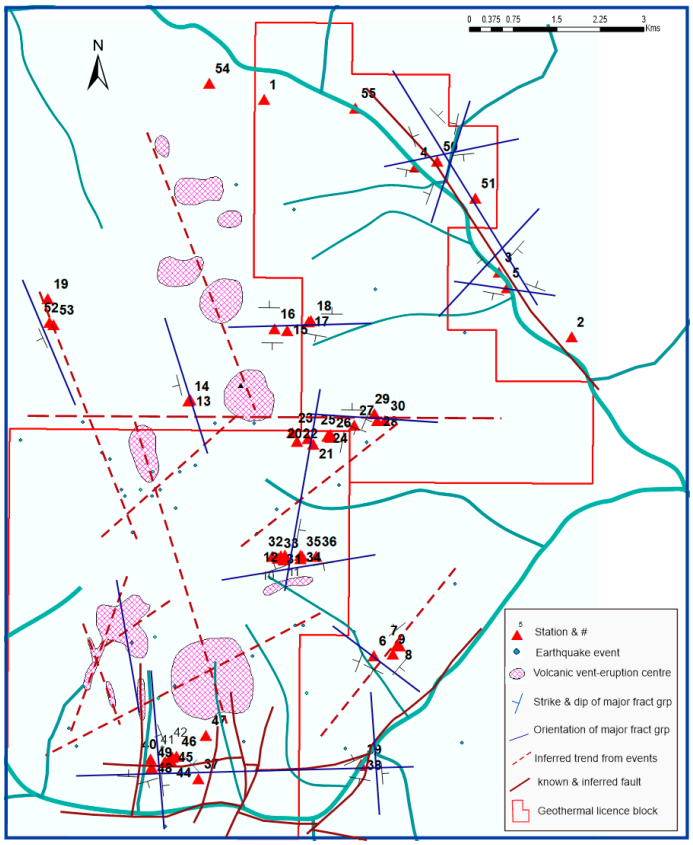

Figure 1. Orientations of major tectonic features interpreted from volcanic eruption centre/vents, recorded earthquake, and known and inferred faults from geophysical data and fracture strike groups. Figure modified from [31].

The MMVC experiences a local stress field influenced by regional tectonics and topography. A prior study utilized existing data to assess how topographical variations combined with tectonic stresses impact the in situ stress field at Mount Meager [33]. At shallow depths of less than 2000 m, a normal faulting regime predominates, with vertical stress as the principal stress. According to Hubbert and Willis [34], vertical fractures will be formed under active normal faulting. The orientations of maximum and minimum horizontal stresses vary locally based on topographic differences. Given that this study was conducted on a regional scale, the fracture plane was modelled as circular to encompass all potential scenarios, as shown in Figure 2.

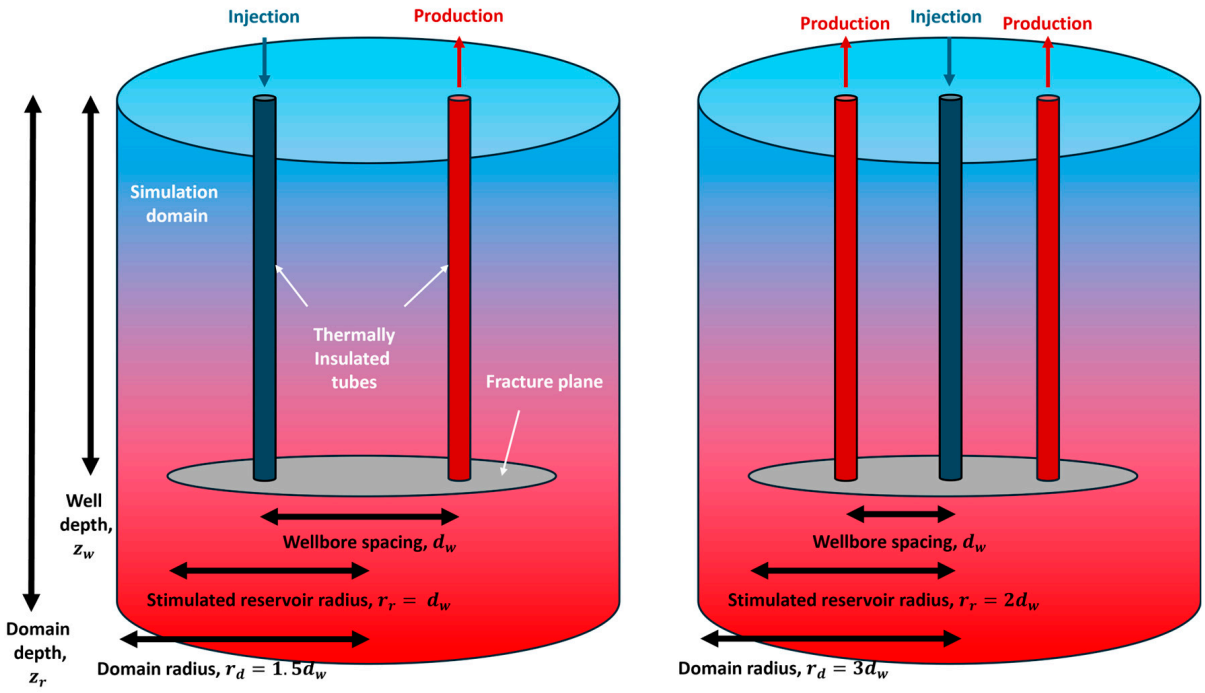

Figure 2. (**a**) Doublet and (**b**) triplet configuration built for the numerical model under the one-fracture case.

2.2. Wellbore Configurations

In this paper, two wellbore placement patterns are examined: doublet and triplet, as illustrated in Figure 2, under various wellbore configurations. For the doublet system, one injector and one producer are positioned alongside each other, with their midpoints located at the centre of the stimulated fracture plane. Both tubes are thermally insulated, ensuring that fluid only enters or exits at the bottom of each wellbore, which intersects the fracture plane where fluid communication occurs between the two wellbores. The domain radius is chosen to be 1.5 times the wellbore spacing to minimize boundary effects on the simulation results, as this setup models an infinite rock mass, without sacrificing the computational efficiency. The shape and orientation of the fracture plane is determined by the in-situ stress field of the rocks. The fracture plane is modelled as a planar feature with a thermally thin approximation, treating it as a 2D entity within a 3D domain. This approximation assumes a uniform temperature across the fracture's thickness and focuses exclusively on variations along its length and width, effectively reducing the computational load while maintaining accuracy in key areas of interest.

In contrast, the triplet system, shown on the right of Figure 2, employs a similar configuration but includes two producers placed surrounding a centrally located injector at the centre of the stimulated fracture. The radius of the stimulated fracture is assumed to

remain constant regardless of change in the wellbore configuration. Detailed geometric parameters for the model are listed in Table 1, which started with base case parameters, followed by modifications made for each special case.

Table 1. Geometric parameters for the model.

Parameter	Unit	Value
Doublet base case at 600 m with one fracture		
Well depth	m	600
Fracture depth	m	600
Domain depth	m	800
Wellbore spacing	m	300
Simulated reservoir radius	m	300
Domain radius	m	450
Modifications for different configurations		
Triplet		
Wellbore spacing	m	150
Two-fracture case		
Fracture depth	m	500/600
Three-fracture case		
Fracture depth	m	500/600/700
Domain depth	m	900

2.3. Governing Equations and Thermal–Hydraulic Coupling

The governing equations for the model are divided into two major categories: fluid flow and heat transfer, within two mediums: the rock matrix and the fracture. All formulations are established under the following assumptions: (1) both the rock formation and the fracture plane are fully saturated; (2) the rock formation and the fracture plane are treated separately, assuming hydraulically equivalent to two uniform porous domains with constant porosity and permeability; (3) under high pressure in the fractured reservoir, fluid is considered to be single-phase; (4) since fluid flow and heat transfer are the primary focus of this paper, the fractures are assumed to remain geomechanically stable, with no changes in aperture size or width (i.e., no expansion or contraction) and no new fractures being generated; and (5) a thermally thin approximation is used to model the fracture, meaning the temperature gradient across its thickness is neglected. The list of nomenclatures can be found in Abbreviations part.

Within the formation rock matrix with low porosity, the fluid flow can be described by mass conservation equation as [34]

$$\frac{\partial(\phi_r \rho_w)}{\partial t} = -\nabla \cdot (\rho_w \boldsymbol{u}) \tag{1}$$

where $\boldsymbol{u}$ can be represented using the momentum equation:

$$\boldsymbol{u} = -\frac{\kappa_r}{\mu_w} \nabla p \tag{2}$$

The heat transfer is governed by the energy conservation equation:

$$\left(\rho_r C_{pr}\right)_{eff} \frac{\partial T}{\partial t} + \rho_w C_{pw} \boldsymbol{u} \cdot \nabla T = -\nabla \cdot \boldsymbol{q} \tag{3}$$

where $\boldsymbol{q}$ can be written as

$$\boldsymbol{q} = -k_{reff} \nabla T \tag{4}$$

where the notation eff means effective term and can be represented as

$$k_{reff} = (1 - \phi_r)k_r + \phi_r k_w \tag{5}$$

$$(\rho_r C_{pr})_{eff} = (1 - \phi_r)\rho_r C_{pr} + \phi_r \rho_w C_{pw} \tag{6}$$

On the other hand, the fluid flow within the fractures also follows Darcy's law, however modified to accommodate the aperture of the fracture:

$$b\frac{\partial\left(\phi_f \rho_w\right)}{\partial t} = -\nabla\cdot(b\rho_w \boldsymbol{v}) \tag{7}$$

where $\boldsymbol{v}$ can be written as

$$\boldsymbol{v} = -\frac{\kappa_f}{\mu_w}\nabla_{tangential} p \tag{8}$$

where k_f is an equation of the aperture [35]:

$$\kappa_f = \frac{b^2}{12} \tag{9}$$

The heat transfer equation for the rock matrix is also modified for the fracture heat flow:

$$b\left(\rho_f C_{pf}\right)_{eff}\frac{\partial T}{\partial t} + b\rho_w C_{pw}\boldsymbol{v}\cdot\nabla_{\text{tangential}} T = -\nabla_{\text{tangential}}\cdot\boldsymbol{q_f} \tag{10}$$

where $\boldsymbol{q_f}$ can be written as

$$\boldsymbol{q_f} = -k_{feff}\nabla T \tag{11}$$

Similarly, k_{feff} and $\left(\rho_f C_{pf}\right)_{eff}$ are represented as

$$k_{feff} = \left(1 - \phi_f\right)k_r + \phi_f k_w \tag{12}$$

$$\left(\rho_f C_{pf}\right)_{eff} = \left(1 - \phi_f\right)\rho_f C_{pf} + \phi_f \rho_w C_{pw} \tag{13}$$

In addition to the governing equations discussed above, it is important to introduce the coupling strategy between thermal–hydraulic (TH) processes used in this study. This coupled effect is applied to three parameters of the circulating water: density ρ_w, viscosity μ_w, and thermal conductivity k_w, as functions of the changing temperature of the fluid [36,37]:

$$\rho_w = 996.9\left(1 - 0.000317(T - 298.15) - 0.00000256(T - 298.15)^2\right. \tag{14}$$

$$\mu_w = 0.00002414 \times 10^{\frac{247.8}{T+133}} \tag{15}$$

$$k_w = -922.47 + 2839.5\frac{T}{T_r} - 1800.7\left(\frac{T}{T_r}\right)^2 + 525.77\left(\frac{T}{T_r}\right)^3 - 73.44\left(\frac{T}{T_r}\right)^4 \tag{16}$$

These equations are valid for temperatures within the range of 0 to 265 °C, which corresponds to the possible formation temperatures that the wellbore fluid will encounter.

To quantify the energy output potential of the geothermal energy extraction, the output thermal power is calculated as

$$P = m_w C_{p,f}\left(T_{prod} - T_{inj}\right) \tag{17}$$

The cumulative produced energy over the lifespan of the well can be expressed with

$$E = \int_0^{t_w} P dt \tag{18}$$

2.4. Initial and Boundary Conditions

This study is constructed for the geothermal exploitation of Mount Meager; therefore, the reservoir properties are induced from the geological studies conducted on-site. Previous studies have confirmed that within the core of South Meager Mountain, the in-situ temperature can reach 200 °C at a shallow depth of 600 m [5]. Linear increase in temperature is assumed from the surface to that depth, where the surface ambient temperature is approximately 11 °C. Below 600 m, the thermal gradient is still linear, but no longer the same slope as above, with more details discussed in the section below.

Throughout the production period, constant injection temperature and injection flow rate are imposed as boundary conditions at the wellhead, while the temperature of the rock and the fracture first align with the in-situ temperature, then drop progressively as the fluid takes away the heat. Initially, the surface pressure and domain boundary pressure are set to zero, whereas the reservoir pressure is determined by an equation accounting for depth, rock density, and gravity. All initial and boundary conditions used for this study are detailed in Table 2.

Table 2. Initial and boundary conditions.

Parameter	Unit	Value
Thermal		
Surface temperature	°C	11
Initial temperature at 600 m	°C	200
Initial temperature at 1200 m	°C	250
Initial temperature at 2000 m	°C	265
Hydraulic		
Surface pressure	MPa	0
Reservoir boundary pressure	MPa	0
Operational		
Injection rate	kg/s	100
Injection temperature	°C	11

The intrinsic properties of the formation rock, in which the stimulated fracture is embedded, are also crucial for this study. At depths greater than 600 m—which marks the shallowest depth of wellbores in our study—the reservoir rock consists of crystalline quartz diorite beneath the volcanic cover [38]. It is assumed that the stimulated fracture plane has a porosity of 1. For simplicity, a constant aperture is maintained throughout this study at 0.1 mm, which is considered reasonable compared to measured apertures from other ongoing geothermal projects in similar geological settings. Table 3 below lists the values used to characterize the rock matrix and the fracture. The values used to represent the circulating fluid, water, are borrowed from the universally accepted standard, considering TH coupling.

Table 3. Properties of formation rock and fracture.

Parameter	Unit	Value
Rock Matrix		
Density	kg/m^3	2700
Heat capacity	J/(kg·K)	1150

Table 3. *Cont.*

Parameter	Unit	Value
Thermal conductivity	W/(m·K)	3.2
Porosity	-	0.01
Permeability	mD	0.1
Fracture		
Density	kg/m^3	2700
Heat capacity	J/(kg·K)	1150
Thermal conductivity	W/(m·K)	3.2
Porosity	-	1
Aperture	mm	0.1

2.5. Mesh Sensitivity

The model utilizes a mesh composed of free tetrahedral elements, with targeted refinements near the fracture plane boundaries and at the intersecting points between the fracture planes and the wellbores. This refined mesh distribution is strategically designed to enhance the model's ability to capture nuanced changes in thermal and fluid dynamics, which are critical for accurately applying the initial and boundary conditions of the simulation.

Figure 3 presents a comparative analysis of production temperatures over the operational period using three distinct mesh configurations. These configurations are defined by their mesh density: the coarse mesh comprises 21,159 elements, the normal mesh 31,897 elements, and the fine mesh 70,767 elements. Visually, the differences between the normal and fine meshes are minimal, especially when the production period exceeds 10 years. This observation is supported statistically, with a mean absolute error of 1.8 °C and a root mean square error of 3 °C between the normal and fine meshes. Consequently, the normal mesh has been chosen for continued use in this study to optimize the balance between simulation accuracy and computational efficiency.

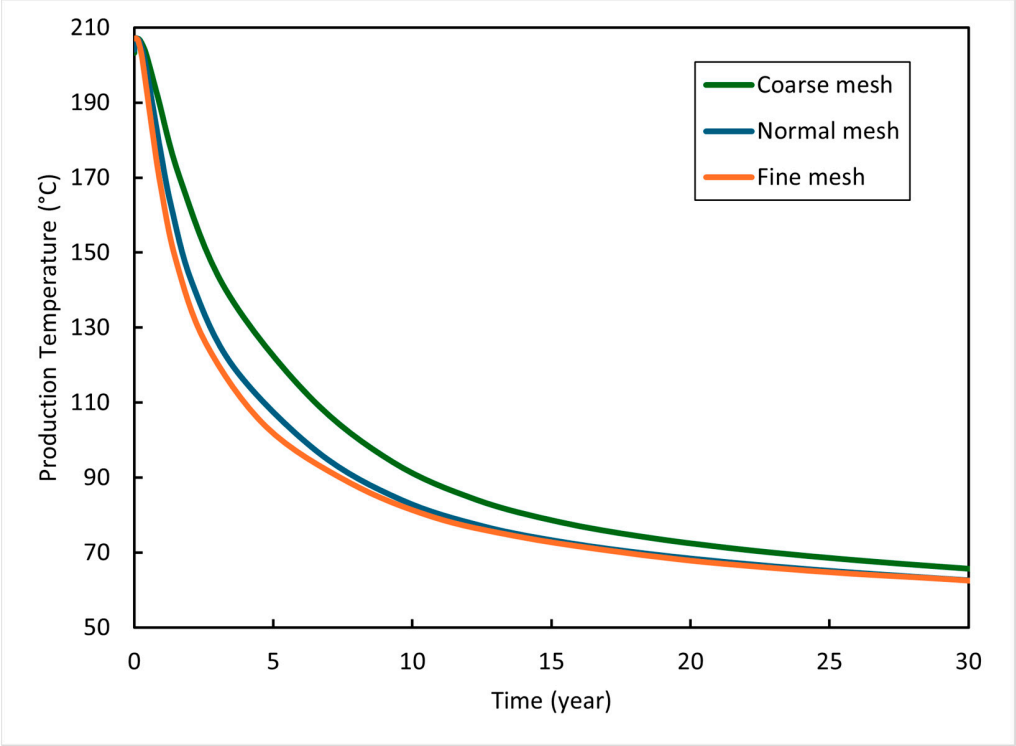

Figure 3. Production temperature over 30 years with varying mesh density.

3. Validation

In order to validate the credibility of the numerical model, here we present an analytical solution that our numerical results are in comparison of. For simplicity, we consider a two-dimensional analytical solution developed by Bodvarsson [39] considering fluid flow and heat transfer in an infinite rock matrix with a single fracture in the middle that connects boundaries on the opposite sides of the rock. The geometry and the parameters used for analytical computations can be found in Figure 4. A steady water injection at the right end of the fracture which sits in the middle of the rock matrix is maintained under constant injection velocity and temperature. The fluid will travel through the fracture until it reaches the output at the left end of the fracture. The reservoir has a constant temperature of 110 °C.

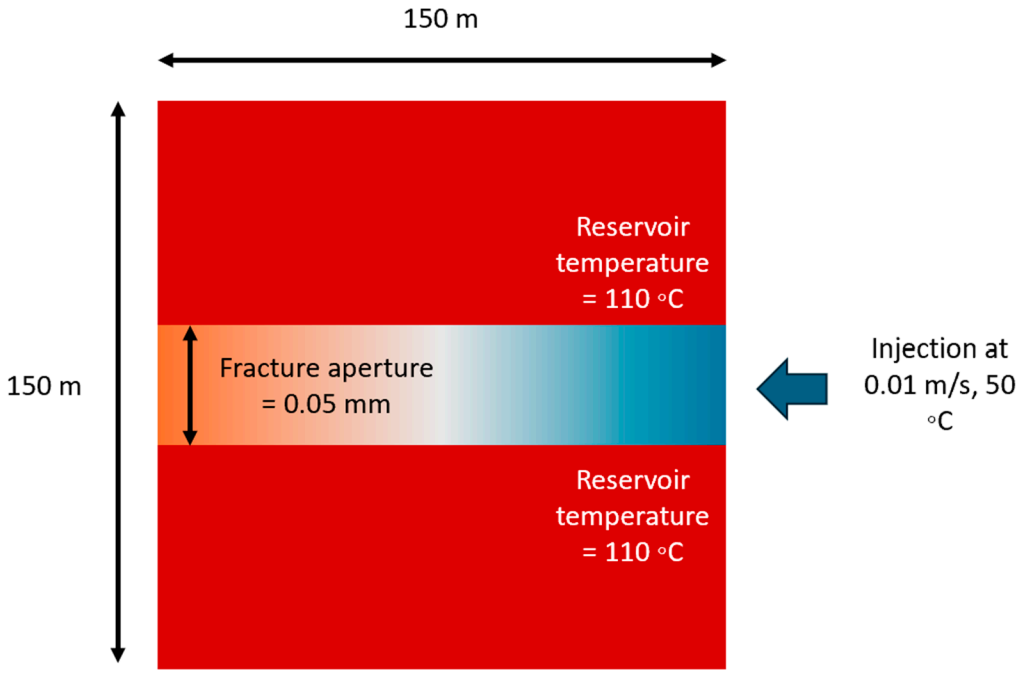

Figure 4. Model configuration for the analytical solution following [16].

The analytical solution is given with the following equation [40]:

$$T_{out} = T_i + (T_{in} - T_i) erfc\left(k_r x / \left(\frac{\rho_f C_{p,f} b}{\sqrt{v_{in}(v_{in}t - x)k_r/(\rho_r C_{p,r})}}\right)\right) U\left(t - \frac{x}{v_{in}}\right) \quad (19)$$

where T_{out} is the temperature at the outlet, T_i is the initial temperature, x is the distance away from the input along the axis parallel to the fracture extension, and v_{in} is the injection velocity. $erfc$ stands for complementary error function and U represents the unit step function.

Figure 5 illustrates the validation of the numerical model presented in this paper by comparing the calculated results with the analytical solution. A reasonable degree of similarity can be observed between the two sets of data, although the numerical results are slightly higher than the analytical solution. The absolute difference is less than 1 °C, demonstrating the validity of the numerical model.

Applying 2D validations to 3D systems has inherent limitations and potential inaccuracies. While this approach enhances computational efficiency, it may overlook complex interactions between the fracture and the surrounding rock matrix, such as heat loss to the sides and intricate fluid dynamics in the third dimension. These interactions are particularly critical in more heterogeneous geological settings where the uniformity assumed by the

2D model does not hold. Furthermore, the generalizability of the 2D model results may be limited. While the model might provide accurate predictions under controlled conditions or within specific parameter ranges, extending these findings to different geological or operational settings could be restricted.

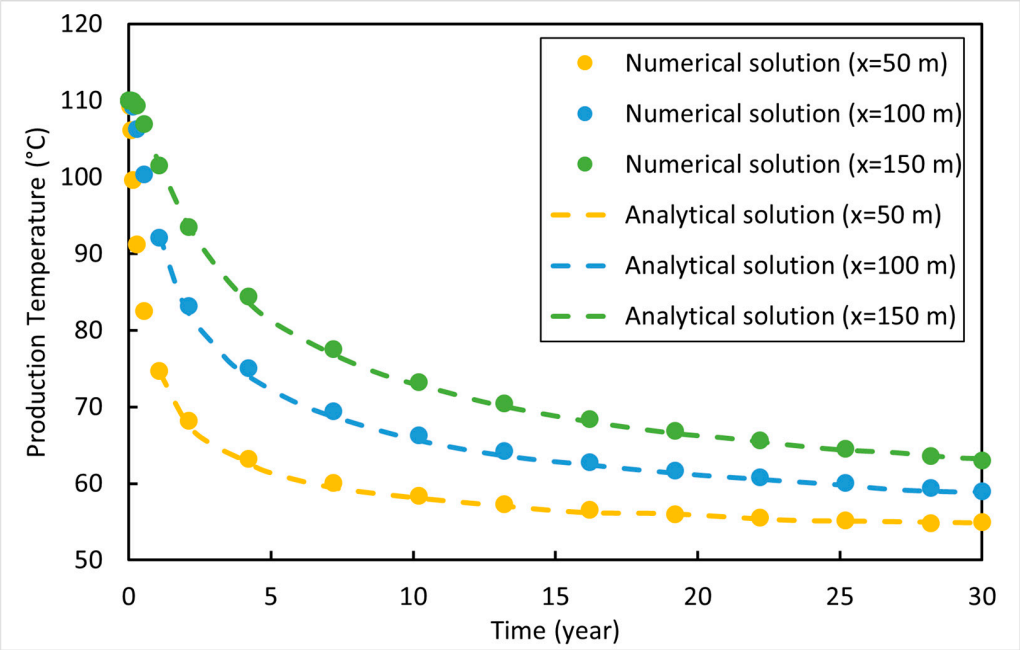

Figure 5. Numerical and analytical results of temperature along the fracture at distance of 50 m, 100 m, and 150 m away from the inlet.

However, under the thermally thin approximation, utilizing 2D validation for modelling 3D simulations of geothermal systems, as discussed in this paper, can be a potentially accurate and efficient method. This approximation simplifies the representation of fractures within a 3D domain by treating them as 2D entities, which is justified when the fracture's thickness is negligible compared to its length and width. This allows for disregarding temperature and pressure gradients across the thickness. In such scenarios, a 2D model can effectively capture the essential dynamics of fluid flow and heat transfer that occur in a real 3D environment, particularly in cases where lateral heat transfer and multi-directional fluid flow are minimal. In addition, given the significant challenges associated with deriving analytical solutions in 3D—often unfeasible due to computational constraints and the complexity of multiphysics interactions—2D validation is employed in this study. This method remains crucial for understanding and predicting geothermal behaviour under specified conditions, while also necessitating the careful consideration of its applicability and limitations.

4. Results

This section is organized as follows: first, we present three studies involving one, two, and three fractures under the base case scenario, where the operational parameters remain constant. These parameters include an injection temperature equal to the surface temperature and an injection rate of 100 kg/s. The stimulated reservoir is also modelled under the base parameters, with a radius of 300 m and a fracture aperture of 0.1 mm. Additionally, the well configuration is a doublet system, consisting of one injector and one producer, with both wells extending to a depth of 600 m. Following the analysis of the base case, we will conduct sensitivity analyses to examine the impacts of these parameters on geothermal energy production.

4.1. Base Case

Figure 6 illustrates the temperature contour of fluid propagation along the fracture plane for the one-fracture case at 500 m deep at different times. Cold fluid is injected from the left side of the fracture plane and extracted from the right side through the producer, gradually harvesting the heat stored in the rock. As shown in Figure 6, after one year into the production, cooling is concentrated near the injector. Over time, the cooling front advances toward the producer until the entire area between the injector and producer reaches the same temperature as the injection fluid, signifying the depletion of the heat in place. As the thermal front approaches the producer, thermal breakthrough intensifies, causing a sharp decline in production temperature during the initial stage, followed by a less rapid decrease in the subsequent years.

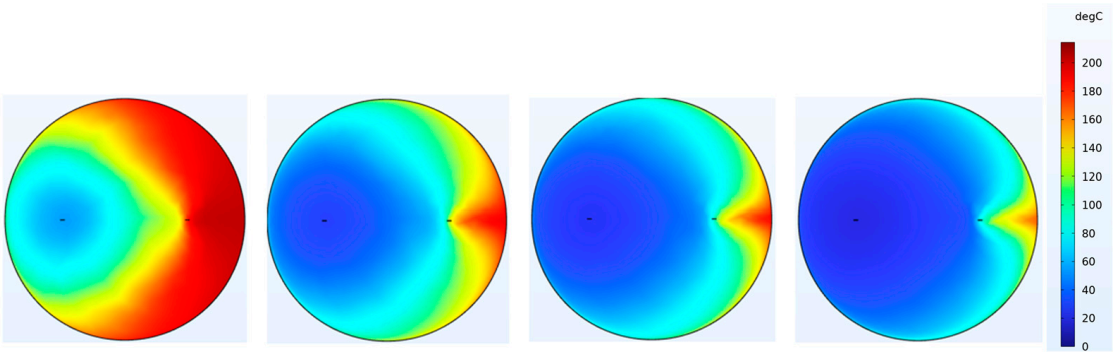

Figure 6. Temperature contour of the fracture plane for the base case with one discrete fracture at the depth of 500 m after 1 year, 5 years, 10 years, and 30 years.

Figure 7 features two discrete fractures at depths of 500 and 600 m. This arrangement allows for a more complex and effective heat transfer process. The additional fracture, located deeper at 600 m, enhances the overall cooling effect by providing a secondary pathway for the thermal front to progress. This not only prevents premature thermal saturation observed in the upper fracture but also supports a more uniform cooling distribution across the plane. Consequently, the system's efficiency in heat extraction is maintained over a longer period, highlighting the benefits of incorporating multiple fractures at varying depths.

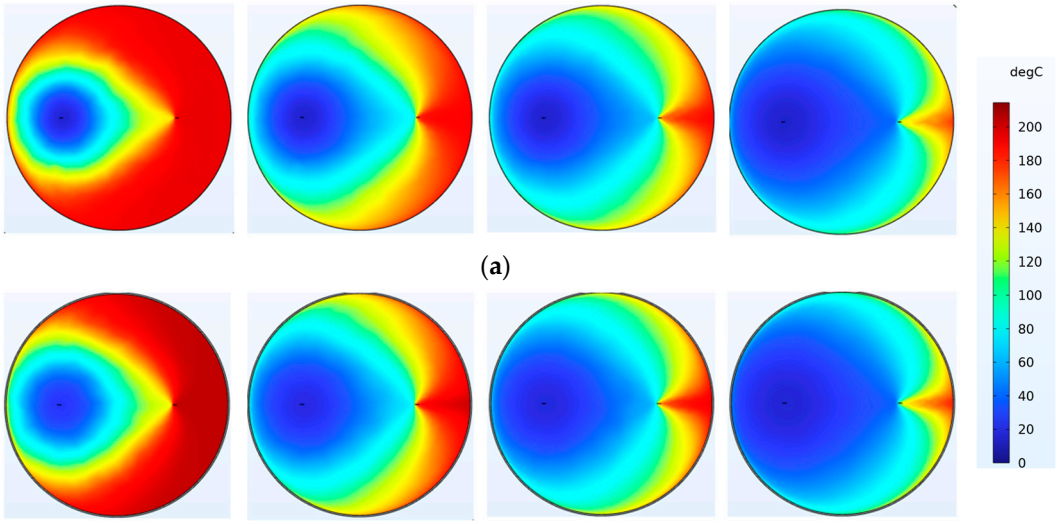

Figure 7. Temperature contour of the fracture plane for the base case with two discrete fractures at depth of (**a**) 500 m, and (**b**) 600 m after 1 year, 5 years, 10 years, and 30 years.

The three-fracture case shown in Figure 8, with three fractures at 400, 500, and 600 m, exhibits the most significant advantages in terms of thermal management and system sustainability. The uppermost fracture at 400 m introduces an early cooling effect, which is particularly effective in managing the heat near the injection site. As the cooling extends deeper to the fractures at 500 and 600 m, it encounters undisturbed heat reservoirs with higher in situ temperatures because of the thermal gradient, which allows for continued effective heat extraction. This staggered arrangement of fractures ensures that the cooling is not only rapid and extensive but also evenly distributed, avoiding the localized overheating and thermal bottlenecks that could hinder the system's performance.

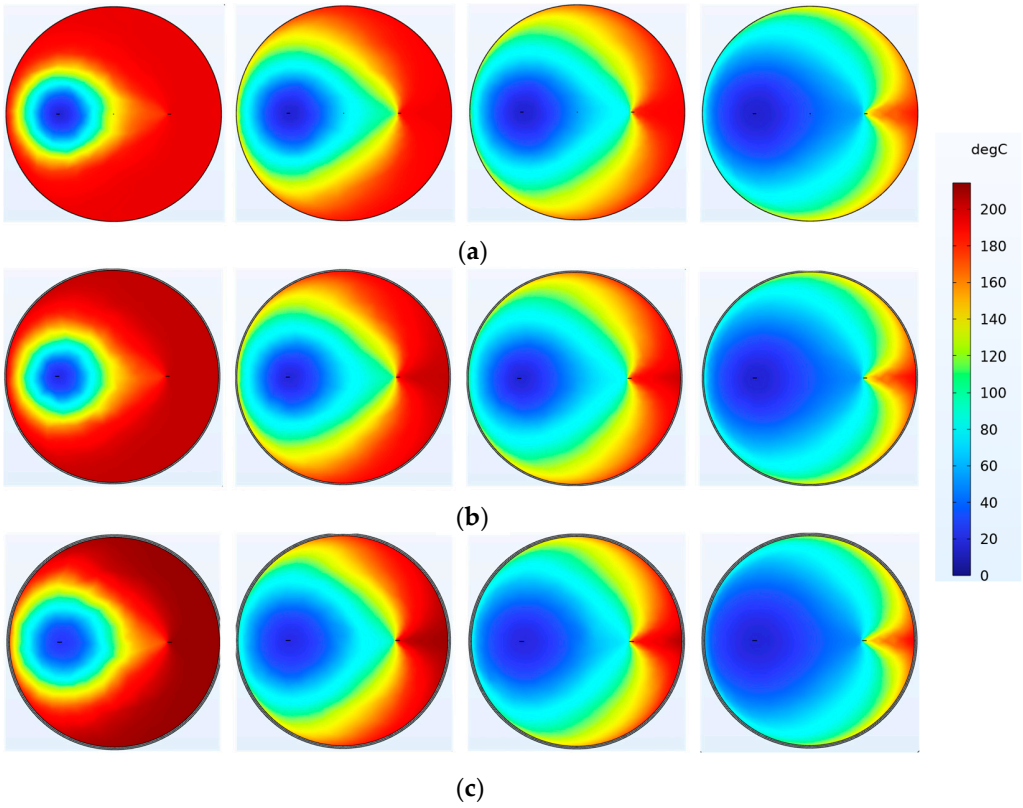

Figure 8. Temperature contour of the fracture plane for the base case with three discrete fractures at depth of (**a**) 400 m, (**b**) 500 m, and (**c**) 600 m after 1 year, 5 years, 10 years, and 30 years.

The above trend is also depicted in Figure 9a, which illustrates the production temperature over a 30-year period for the different fracture configurations. The production temperature decreases over time, as expected, due to the cooling of the reservoir as thermal energy is extracted. The system with three fractures initially exhibits the highest production temperature, starting at approximately 215 °C, followed by the two-fracture system at around 210 °C, and the one-fracture system at 205 °C. This is due to the fact that the additional fracture planes are progressively deeper than the one above, therefore resulting in a higher in-situ temperature due to thermal gradient. By the end of the 30-year period, the production temperature has declined to approximately 120 °C for the three-fracture system, 105 °C for the two-fracture system, and 95 °C for the one-fracture system. These results demonstrate that the system with three fractures maintains a production temperature that is about 26% higher than the one-fracture system at the 30-year mark. This significant difference highlights the importance of increasing the number of fractures to enhance heat extraction efficiency, as the additional fractures provide a larger surface area for heat exchange, allowing for more sustained temperature levels.

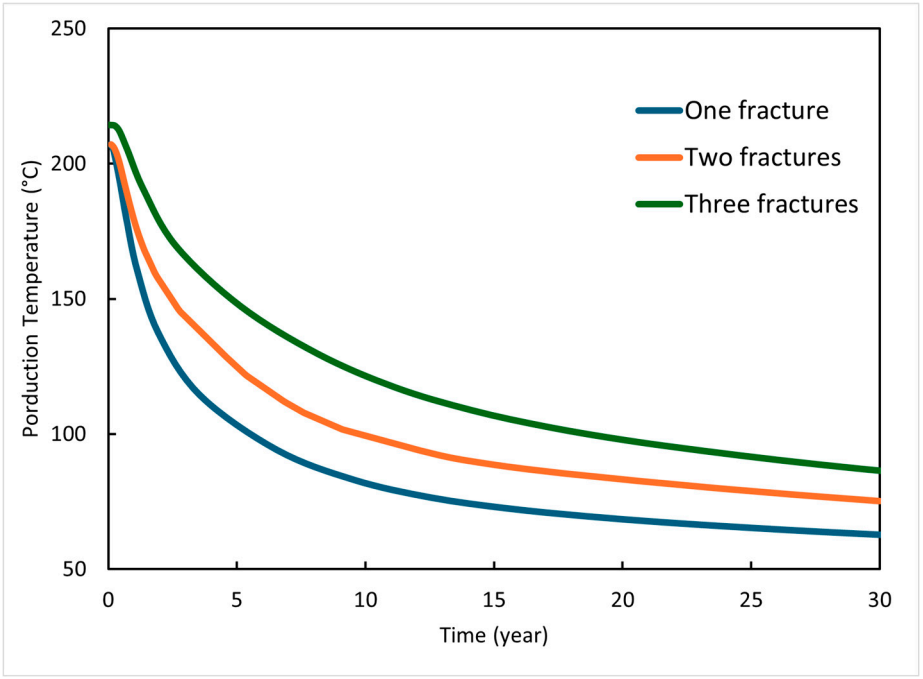

(**a**)

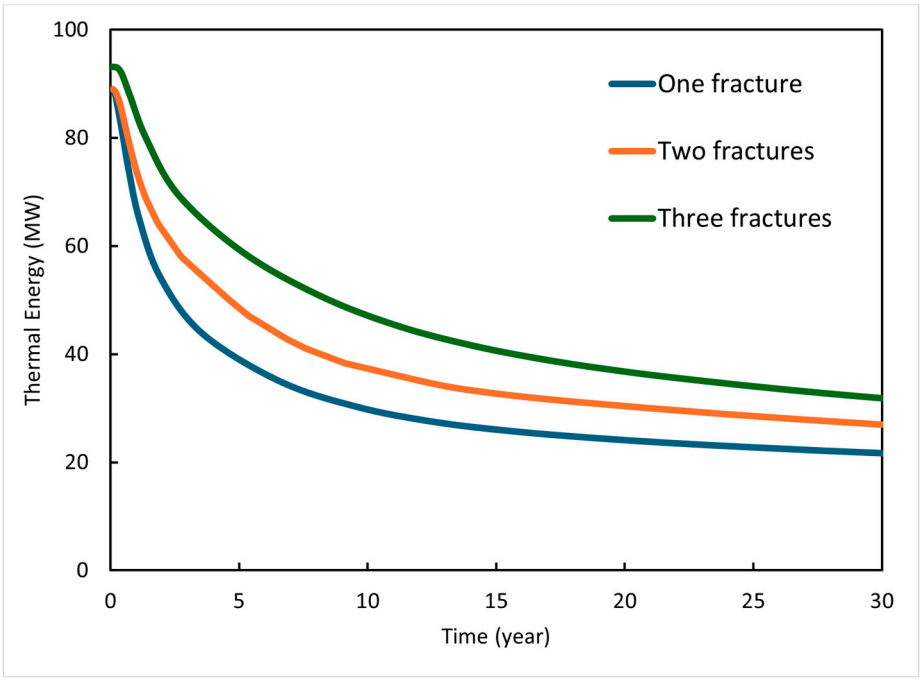

(**b**)

Figure 9. (**a**) Production temperature and (**b**) thermal energy produced from the base case simulation with one, two, and three stimulated fracture planes.

Figure 9b focuses on thermal energy output over time, an equally critical parameter that directly reflects the system's efficiency in converting reservoir heat into usable energy. The maximum thermal energy output at the beginning of the simulation is approximately 95 MW for the three-fracture system, 85 MW for the two-fracture system, and 75 MW for the one-fracture system. Over time, the thermal energy output decreases, with the three-fracture system maintaining the highest output throughout the simulation period. By the end of the 30-year period, the thermal energy production for the system with three fractures is approximately 50% greater than that of the one-fracture system. This difference

underscores the enhanced efficiency provided by additional fractures, which allow for a more extensive heat exchange area and consequently higher thermal energy production under higher efficiency.

4.2. Sensitivity Analysis on Operational Parameters

This section presents a sensitivity analysis of key operational parameters using our model, focusing specifically on the injection temperature and injection rate. Understanding how variations in these parameters influence the system's performance is crucial for optimizing geothermal energy extraction. By systematically altering the injection temperature and injection rate while keeping reservoir characteristics and well configurations constant, we aim to quantify their impacts on the overall energy production.

4.2.1. Injection Rate

Figure 10 illustrates the relationship between cumulative produced energy and injection rate for systems with one, two, and three fractures. The cumulative produced energy increases with higher injection rates across all fracture configurations. At an injection rate of 50 kg/s, the cumulative produced energy is approximately 20.47$\times$ 10^6 GJ for the one-fracture system, 26.18 $\times$ 10^6 GJ for the two-fracture system, and 29.89 $\times$ 10^6 GJ for the three-fracture system. As the injection rate increases to 500 kg/s, these values rise significantly, reaching approximately 68.64 $\times$ 10^6 GJ for the one-fracture system, 85.86 $\times$ 10^6 GJ for the two-fracture system, and 97.02 $\times$ 10^6 GJ for the three-fracture system.

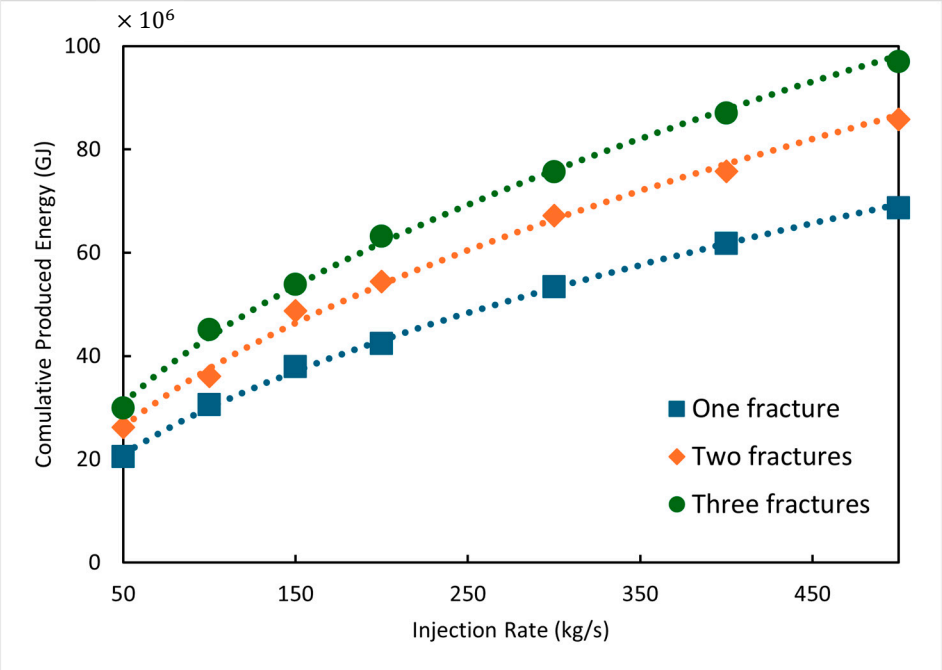

Figure 10. Cumulative production energy over 30-year operational time with varying injection rates for one, two, and three fractures.

The incremental increase in cumulative produced energy with respect to injection rate is also noteworthy. For each fracture configuration, the energy output shows a power relationship with injection rate, with exponent equals to approximately 0.5 for all three cases. The system with three fractures consistently outperforms the other configurations, producing approximately 41% more energy at 500 kg/s compared to the one-fracture system and about 13% more than the two-fracture system at the same injection rate.

4.2.2. Injection Temperature

Figure 11 shows the relationship between cumulative produced energy and injection temperature for systems with one, two, and three fractures. The cumulative produced energy decreases as the injection temperature increases across all fracture configurations. At a lower injection temperature of 11 °C, the cumulative produced energy is approximately 31.04×10^6 GJ for the one-fracture system, 39.22×10^6 GJ for the two-fracture system, and 45.56×10^6 GJ for the three-fracture system. As the injection temperature increases to 60 °C, these values decrease to around 18.83×10^6 GJ for the one-fracture system, 24.30×10^6 GJ for the two-fracture system, and 30.22×10^6 GJ for the three-fracture system.

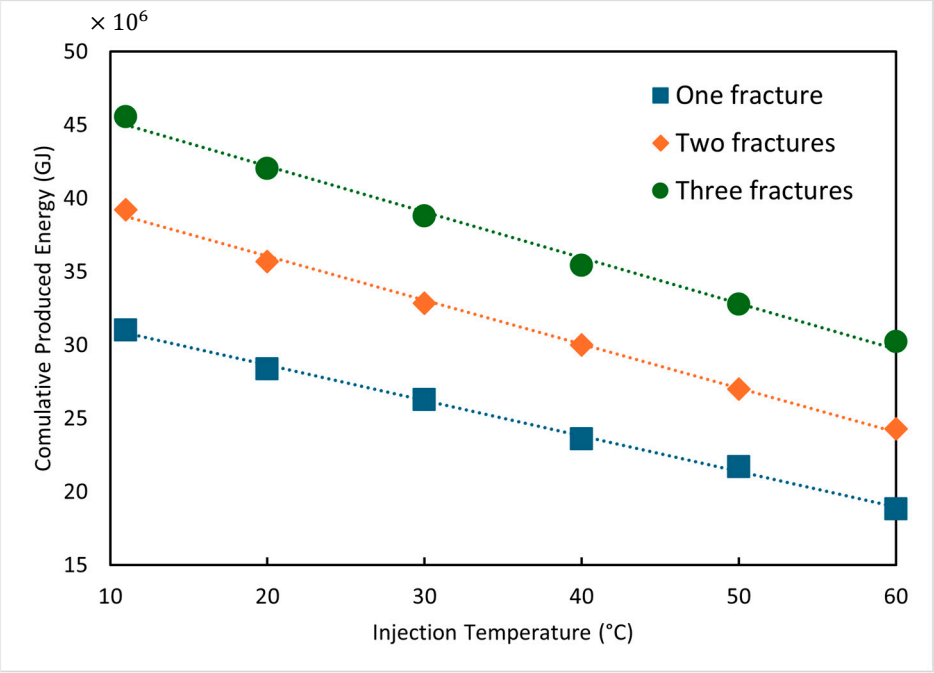

Figure 11. Cumulative production energy over 30-year operational time with varying injection temperatures for one, two, and three fractures.

The decline in cumulative produced energy with increasing injection temperature is notable across all scenarios. The reduction in energy output as the injection temperature increases is linear, with the three-fracture system consistently producing the highest cumulative energy. For instance, at an injection temperature of 11 °C where the maximum energy is produced, the energy produced by the three-fracture system is approximately 47% higher than that produced by the one-fracture system. Additionally, the energy produced by the two-fracture system is about 31% higher than the one-fracture system under the same conditions.

4.3. Sensitivity Analysis on Reservoir Characteristics

This section explores the sensitivity analysis of stimulated reservoir characteristics, with a particular emphasis on the fracture radius. The fracture radius is a critical parameter that influences the efficiency of geothermal energy extraction by determining the extent of the heat exchange surface within the reservoir. Theoretically, reservoir characteristics such as radius and aperture are not flexible parameters that can be altered by engineers; rather, they are determined by the geomechanics properties of the undisturbed reservoir rocks and the in-situ stress state. Since we currently lack a comprehensive understanding of these factors, designing around them is beyond the scope of this paper. Therefore, a

sensitivity analysis is conducted to evaluate energy production under various scenarios, offering guidance for potential future stimulation strategies.

Figure 12 illustrates the relationship between cumulative produced energy and wellbore spacing, which serves as a proxy for the fracture radius. As the wellbore spacing increases, representing a larger fracture radius, the cumulative produced energy also increases across all fracture configurations. At a wellbore spacing of 50 m, the cumulative produced energy is approximately 5.853×10^6 GJ for the one-fracture system, 8.557×10^6 GJ for the two-fracture system, and 11.41×10^6 GJ for the three-fracture system. When the wellbore spacing increases to 300 m, these values rise significantly to around 61.99×10^6 GJ for the one-fracture system, 70.98×10^6 GJ for the two-fracture system, and 78.83×10^6 GJ for the three-fracture system.

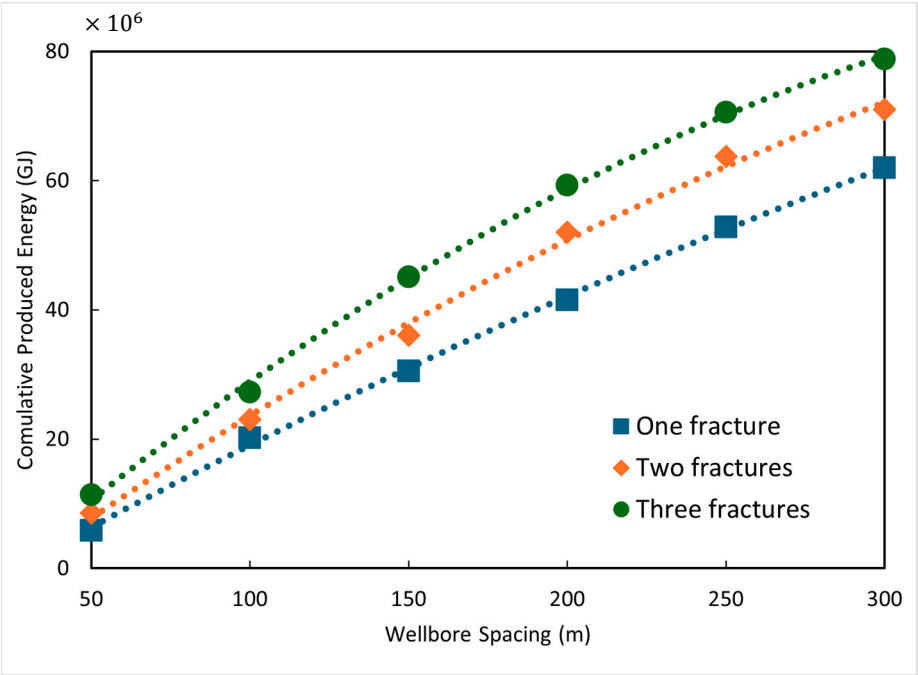

Figure 12. Cumulative production energy over 30-year operational time with varying reservoir radius for one, two, and three fractures.

The increase in cumulative-produced energy with larger wellbore spacing indicates that a greater fracture radius enhances the heat exchange surface area, leading to more effective thermal energy extraction. The rate of energy production increase is relatively linear, with the three-fracture system consistently yielding the highest cumulative energy. At a wellbore spacing of 300 m, the energy produced by the three-fracture system is approximately 27% higher than that produced by the one-fracture system, and about 11% more than the two-fracture system.

4.4. Sensitivity Analysis on Wellbore Configuration

This section investigates the sensitivity of geothermal system performance to variations in wellbore configurations, focusing on well depth and the well patterns. At Mount Meager, the thermal gradient does not increase linearly with depth; previous studies have shown that the rock mass temperature can reach 250 °C at a depth of 1200 m, increasing to 265 °C at a depth of 2000 m. Additionally, we will examine the impact of wellbore placement, specifically comparing the performance of doublet and triplet systems, as discussed in the previous section.

4.4.1. Wellbore Depth

Figure 13 illustrates the relationship between cumulative produced energy and well depth for systems with one, two, and three fractures. As the well depth increases, representing greater access to higher temperatures in the geothermal reservoir, the cumulative produced energy also increases across all fracture configurations. At a well depth of 600 m, the cumulative produced energy is approximately 29.92 $\times$ 10^6 GJ for the one-fracture system, 38.74 $\times$ 10^6 GJ for the two-fracture system, and 45.09 $\times$ 10^6 GJ for the three-fracture system. When the well depth increases to 2000 m, these values rise to around 47.75 $\times$ 10^6 GJ for the one-fracture system, 54.84 $\times$ 10^6 GJ for the two-fracture system, and 62.32 $\times$ 10^6 GJ for the three-fracture system.

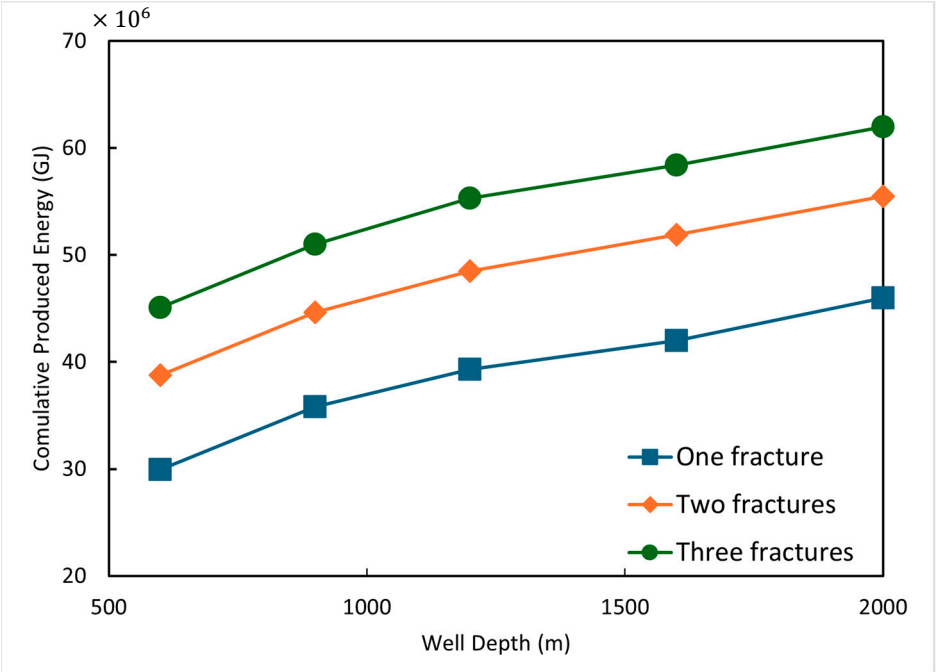

Figure 13. Cumulative production energy over 30-year operational time with varying well depth for one, two, and three fractures.

The increase in cumulative-produced energy with greater well depth aligns with the observed higher temperatures at deeper levels within the Mount Meager geothermal reservoir. This trend is consistent across all fracture configurations, with the three-fracture system consistently producing the highest cumulative energy. At a well depth of 2000 m, the energy produced by the three-fracture system is about 35% higher than that of the one-fracture system, and approximately 12% more than the two-fracture system.

4.4.2. Well Pattern

Figure 14 compares cumulative-produced energy across different wellbore configurations—doublet and triplet—highlighting the impact of well pattern in systems with one, two, and three fractures. In doublet configurations, energy production is notably lower, with the one-fracture system generating approximately 30.23 $\times$ 10^6 GJ, the two-fracture system around 35.65 $\times$ 10^6 GJ, and the three-fracture system approximately 45.09 $\times$ 10^6 GJ. Transitioning to triplet configurations, there is a marked increase in energy output: the one-fracture system jumps to about 42.33 $\times$ 10^6 GJ, showing a 40% enhancement, the two-fracture system escalates to roughly 47.96 $\times$ 10^6 GJ with a 35% enhancement, and the three-fracture system peaks at around 60.04 $\times$ 10^6 GJ, representing a 33% increase over their doublet counterparts. This substantial boost in energy production with the triplet configuration

suggests its superior efficiency in facilitating a more extensive and effective heat exchange area, thus allowing for a higher volume of geothermal fluid circulation and enhanced access to the reservoir's heat resources.

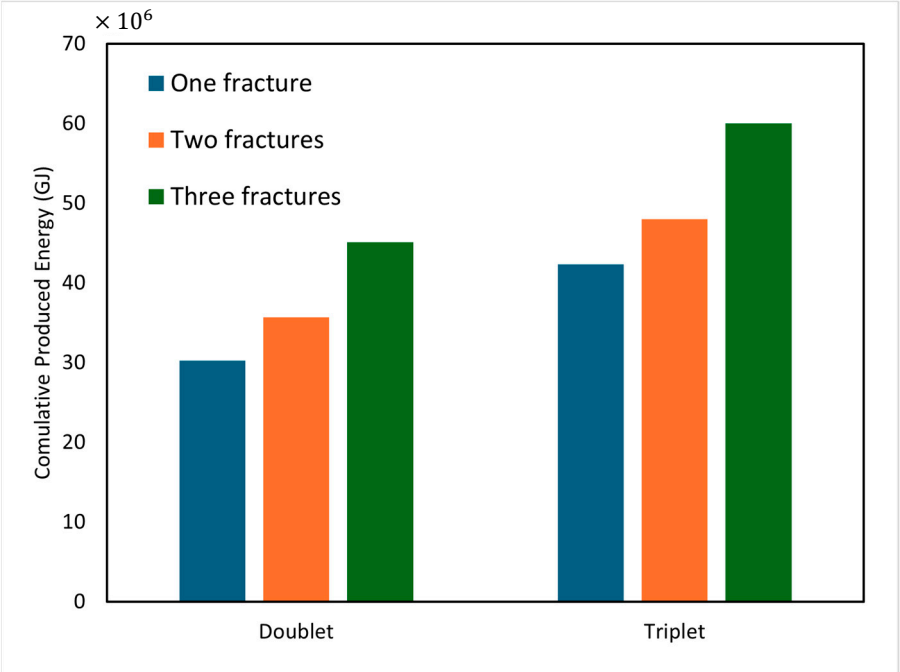

Figure 14. Cumulative production energy over 30-year operational time under different wellbore patterns for one, two, and three fractures.

5. Discussion

The sensitivity analyses conducted across various parameters—operational settings, reservoir characteristics, and wellbore configurations—offer important insights into the optimization of geothermal energy systems. This discussion synthesizes these findings by exploring their correlations and future implementation at Mount Meager, providing a comprehensive overview that guides the enhancement of system performance.

Operational parameters such as injection rate and temperature play critical roles in system efficiency. The analysis revealed a power–law relationship between higher injection rates and increased cumulative energy production across different fracture configurations. For example, increasing the injection rate from 50 kg/s to 450 kg/s resulted in up to a 224% increase in cumulative energy production in systems with three fractures. However, this approach requires balancing to avoid rapid resource depletion and thermal breakthrough. In contrast, higher injection temperatures were found to decrease energy production, affirming the principle that cooler injection fluids more effectively exploit the reservoir's thermal gradient. Specifically, as injection temperatures increased from 11° C to 60 °C, there was a consistent reduction in cumulative energy output by approximately 35% across all configurations. One major assumption being made here is that the injected water is sourced from the surrounding environment. However, in reality, the recirculating water will come from the fluid leaving the Organic Rankine Cycle (ORC) or another electricity generation facility, which means that the temperature of the water as it exits the facility will be higher than the surface temperature. Unless time and space are allowed for the water to cool down, this could lead to higher operational costs associated with additional water-cooling facilities. Thus, optimizing injection rates while controlling injection temperatures can significantly enhance both performance and sustainability of the geothermal operation.

In terms of reservoir characteristics, larger wellbore spacing, serving as a proxy for fracture radius, was associated with enhanced cumulative energy production. Increasing spacing from 50 m to 300 m led to an 590% increase in energy output for systems with three fractures. This suggests that expanding fracture radii which is directly associated with the surface area for heat extraction could effectively increase the heat exchange surface area, improving thermal recovery. Practical applications might include the development of fracturing techniques that safely increase fracture radii, thereby boosting performance while complying with the geomechanics conditions of the reservoir.

Deeper well depths correlated with higher energy outputs due to the access to higher temperatures available at greater depths, supporting the practice of targeting deeper reservoir zones in regions with favourable geothermal gradients. Quantitatively, deeper wells accessed higher temperatures, resulting in a 37% increase in energy production when well depths were extended from 600 m to 2000 m for the three-fracture system. Additionally, triplet configurations outperformed doublets, indicating that adding more wells in proximity can lead to better interconnectivity between fractures and enhanced fluid circulation.

The interdependencies between these parameter groups highlight the complexity of geothermal system optimization. For example, while higher injection rates and a higher number of wells both contribute to increased energy production, their benefits must be weighed against increased costs and potential geological limits. Moreover, while deeper wells access higher temperatures, the economic and technical feasibility of such drilling must be considered.

6. Conclusions

This paper provides a feasibility study for geothermal exploitation at Mount Meager utilizing an enhanced geothermal study, emphasizing the critical impact of various operation parameters, reservoir characteristics, and wellbore configurations on the geothermal energy extraction. Our findings confirm that the unique geological setting of Mount Meager, characterized by high in-situ temperatures at relatively shallow depths, presents a significant opportunity for geothermal development. Notably, under one of the best-case scenarios simulated in the study, there is potential to produce 60 $\times 10^6$ GJ of energy over 30 years of production. This optimal scenario involves a triplet system with three stimulated fracture planes, injecting fluid at a rate of 100 kg/s at surface temperature. The energy production can be further improved, using the key findings summarized from the sensitivity analyses performed:

- Increased injection rates result in significantly higher cumulative-produced energy, particularly in systems with multiple fractures. However, higher injection temperatures decrease energy production, affirming the effectiveness of cooler injections.
- Larger wellbore spacings, indicative of increased fracture radii, correlate with increased cumulative energy production, emphasizing the benefits of expanded heat exchange surfaces. Similarly, deeper wells enhance energy output due to access to higher reservoir temperatures.
- Triplet configurations outperform doublets by facilitating more extensive heat exchange areas and improved geothermal fluid circulation, thereby enhancing overall system performance.

The results from this study are based on several key assumptions, detailed in the methodology section, along with potential limitations introduced for the sake of simplicity, as outlined below. This study assumes that the wellbore will encounter isotropic and homogeneous materials, where the properties of the rock remain consistent regardless of location or depth. Additionally, the creation of the fracture plane is presumed due to lack of

data, based on the current understanding of in-situ stress conditions and geomechanics. In reality, the formation of such a fracture plane cannot be guaranteed, and thus the accurate properties of the fracture reservoir remain uncertain. Moreover, the number, geometry, and aperture of the fractures are likely to be altered by the continuous injection of cold fluid—a factor that this study neglects. These assumptions and limitations will be addressed in future studies.

To optimize the systems, several strategies are recommended. Controlled injection strategies can optimize the rate to maximize heat extraction without causing thermal breakthrough, and advanced modelling tools can help predict optimal rates that balance energy production with long-term sustainability. Lowering injection temperatures can exploit the natural thermal gradient more effectively, especially in systems where the geothermal gradient is high. Advanced fracturing technologies, such as multistage fracturing and the use of sophisticated gas compositions, can increase well costs by 5% to 10%, although they may boost gas reserves by 10% to 20% [41]. Continued exploration of deeper well depth in geothermal hotspots is also advised to achieve higher energy production, but the financial and technological investments required should be carefully evaluated, as discussed in works like [42]. Lastly, given the better performance of triplet well configurations over doublet, further research and pilot projects should explore their feasibility and efficiency in various geological settings. Integrating these insights into geothermal project planning and operations can significantly improve outcomes by designing more effective, efficient, and sustainable geothermal energy systems.

Author Contributions: Implementation and writing, Y.C.; supervision, Z.C., W.Y. and S.Y. All authors have read and agreed to the published version of the manuscript.

Funding: The financial support of the Natural Sciences and Engineering Research Council of Canada (NSERC) is gratefully acknowledged.

Data Availability Statement: Data are available upon request due to restrictions.

Acknowledgments: The support of the Natural Sciences and Engineering Research Council of Canada (NSERC) is greatly acknowledged. We thank two anonymous journal reviewers for their helpful comments and suggestions that greatly improved the quality of the paper.

Conflicts of Interest: The authors declare no conflicts of interest.

Abbreviations

List of Nomenclature
Latin letters:

u	Darcy velocity of the water within the rocks ($\frac{m}{s}$)
v	Darcy velocity within the fracture ($\frac{m}{s}$)
C_{pr}	heat capacity of the rock ($\frac{J}{kg \cdot K}$)
C_{pw}	heat capacity of water ($\frac{J}{kg \cdot K}$)
q	conductive heat flux of rock ($\frac{W}{m^2}$)
b	fracture aperture (m)
C_{pf}:	heat capacity of the fracture ($\frac{J}{kg \cdot K}$)
q_f:	conductive heat flux between water and fracture ($\frac{W}{m^2}$)
k_w	thermal conductivity of water ($\frac{W}{m \cdot K}$)
P	output thermal power (W)
m_w:	injection flow rate of the fluid ($\frac{kg}{s}$)
T_{prod}	production temperature (K)
T_{in}	injection temperature (K)
E	cumulative produced energy (J)
t_w	production time (s)

Greek letters:	
ϕ_r	porosity of the formation rock (-)
ρ_w	density of water ($\frac{kg}{m^3}$)
μ_w	dynamic viscosity of water ($Pa{\cdot}s$)
ρ_r	density of the rock ($\frac{kg}{m^3}$)
ϕ_f	porosity of the fracture (-)
κ_r	permeability of rock (m^2)
κ_f	permeability of the fracture (m^2)
ρ_f	density of the fracture ($\frac{kg}{m^3}$))
Operators and notation:	
∇p	pressure gradient (Pa)
∇T	temperature difference (K)

References

1. Grasby, S.E.; Allen, D.M.; Bell, S.; Chen, Z.; Ferguson, G.; Jessop, A.; Kelman, M.; Ko, M.; Majorowicz, J.; Moore, M.; et al. *Geothermal Energy Resource Potential of Canada*; Geological Survey of Canada: Ottawa, ON, Canda, 2012; p. 6914.
2. Becker, W.; Christensen, D.; Cutler, D.; Maguire, J.; McCabe, K.; Reese, S.; Speake, A. Technoeconomic Design of a Geothermal-Enabled Cold Climate Zero Energy Community. *J. Energy Resour. Technol.* **2021**, *143*, 100902. [CrossRef]
3. Witter, J. *South Meager Geothermal Project:New Perspectives from Recently Unearthed Data*; Innovate Geothermal Ltd.: Vancouver, BC, Canada, 2019.
4. Grasby, S.E.; Ansari, S.M.; Barendregt, R.W.; Borch, A.; Calahorrano-DiPatre, A.; Chen, Z.; Craven, J.A.; Dettmer, J.; Gilbert, H. *Garibaldi Geothermal Energy Project—Phase 1*; Geoscience BC: Vancouver, BC, Canada, 2021.
5. Chen, Z.; Grasby, S.E.; Yuan, W.; Liu, X. Ground Surface Temperature Monitoring Data Analysis and Applications to Geothermal Exploration in Volcanic Areas, Mount Meager, Western Canada. *Geothermics* **2023**, *108*, 102610. [CrossRef]
6. Lewis, T.J.; Souther, J.G. *Meager Mountain, B.C.: A Possible Geothermal Energy Resource*; Geothermal series; Energy, Mines and Resources Canada, Earth Physics Branch: Ottawa, ON, Canada, 1978.
7. Chandrasekharam, D. Enhanced Geothermal Systems (EGS) for UN Sustainable Development Goals. *Discov. Energy* **2022**, *2*, 4. [CrossRef]
8. *The Future of Geothermal Energy: Impact of Enhanced Geothermal Systems (EGS) on the United States in the 21st Century: An Assessment*; Massachusetts Institute of Technology, Ed.; Massachusetts Institute of Technology: Cambridge, MA, USA, 2006; ISBN 978-0-615-13438-3.
9. Tester, J.W.; Anderson, B.J.; Batchelor, A.S.; Blackwell, D.D.; DiPippo, R.; Drake, E.M.; Garnish, J.; Livesay, B.; Moore, M.C.; Nichols, K.; et al. Impact of Enhanced Geothermal Systems on US Energy Supply in the Twenty-First Century. *Philos. Trans. A Math. Phys. Eng. Sci.* **2007**, *365*, 1057–1094. [CrossRef]
10. Huenges, E. 25—Enhanced Geothermal Systems: Review and Status of Research and Development. In *Geothermal Power Generation*; DiPippo, R., Ed.; Woodhead Publishing: Sawston, UK, 2016; pp. 743–761. ISBN 978-0-08-100337-4.
11. Nakagawa, M.; Jahanbakhsh, K.; Arshad, M. *Beyond Hydrocarbon Extraction: Enhanced Geothermal Systems*; Springer: Cham, Switzerland, 2016; pp. 487–506. ISBN 978-3-319-40122-5.
12. Fabbri, H.; Sánchez, M.; Maedo, M.; Guimarães, L.; Manzoli, O.L. Numerical Modeling of Fractures Interaction for EGS. *Symp. Energy Geotech.* **2023**, 1–2. [CrossRef]
13. McLean, M.L.; Espinoza, D.N.; Ahmmed, B. Evolution of Hydraulic Fracture Permeability in EGS Considering Natural Fracture Compressibility and Strength of the Surrounding Rock. In Proceedings of the 58th U.S. Rock Mechanics/Geomechanics Symposium, Golden, CO, USA, 23–26 June 2024; p. 2968.
14. COMSOL. COMSOL Multiphysics Reference Manual. Available online: https://doc.comsol.com/5.5/doc/com.comsol.help.comsol/COMSOL_ReferenceManual.pdf (accessed on 16 September 2024).
15. Al-Khoury, R.; Bonnier, P.G.; Brinkgreve, R.B.J. Efficient Finite Element Formulation for Geothermal Heating Systems. Part I: Steady State. *Int. J. Numer. Methods Eng.* **2005**, *63*, 988–1013. [CrossRef]
16. Hu, X.; Banks, J.; Guo, Y.; Liu, W.V. Utilizing Geothermal Energy from Enhanced Geothermal Systems as a Heat Source for Oil Sands Separation: A Numerical Evaluation. *Energy* **2022**, *238*, 121676. [CrossRef]
17. ANSYS FLUENT 12.0 User's Guide. Available online: https://www.afs.enea.it/project/neptunius/docs/fluent/html/ug/main_pre.htm (accessed on 16 September 2024).
18. Luo, F.; Xu, R.-N.; Jiang, P.-X. Numerical Investigation of Fluid Flow and Heat Transfer in a Doublet Enhanced Geothermal System with CO2 as the Working Fluid (CO2–EGS). *Energy* **2014**, *64*, 307–322. [CrossRef]

19. Mategaonkar, M. Chapter 14—Numerical Modeling of Groundwater Flow and Contaminant Transport. In *Groundwater Contamination in Coastal Aquifers*; Senapathi, V., Sekar, S., Viswanathan, P.M., Sabarathinam, C., Eds.; Elsevier: Amsterdam, The Netherlands, 2022; pp. 181–189. ISBN 978-0-12-824387-9.
20. Zeinali, L.; Ehlig-Economides, C.; Nikolaou, M. Enhanced Geothermal System Model for Flow through a Stimulated Rock Volume. In Proceedings of the SPE Annual Technical Conference and Exhibition, Dubai, United Arab Emirates, 21–23 September 2021; OnePetro: Richardson, TX, USA.
21. Chong, Q.; Wang, J.; Gates, I.D. Evaluation of Energy Extraction from a Geothermal Resource in Central Alberta, Canada Using Different Well Configurations. *Geothermics* **2021**, *96*, 102222. [CrossRef]
22. Zhang, X.; Huang, Z.; Li, G.; Wu, X.; Wang, T.; Zhou, X. Enhancing Reservoir Stimulation and Heat Extraction Performance for Fractured Geothermal Reservoirs: Utilization of Novel Multilateral Wells. *Energy* **2024**, *291*, 130410. [CrossRef]
23. Wu, B.; Lei, Z.; Zhao, G.; Jia, S.; Zhang, X.; Jeffrey, R.G. An Efficient Model for Predicting Heat Extraction from a Multiple-Well Enhanced Geothermal System in the Presence of Areal Flow. *Appl. Therm. Eng.* **2022**, *210*, 118399. [CrossRef]
24. Zhang, Q.; Dahi Taleghani, A. Intelligent Fluid Flow Management for Enhanced Geothermal System in Fractured Horizontal Wells. *Appl. Therm. Eng.* **2024**, *239*, 122191. [CrossRef]
25. Kumar, D.; Ghassemi, A. *Hydraulic Stimulation of Multiple Horizontal Wells for EGS Reservoir Creation*; The University of Oklahoma: Norman, OK, USA, 2016.
26. Nassereddine, A.; Zerpa, L.E. On the Feasibility of Deep Geothermal Wells Using Numerical Reservoir Simulation. *Processes* **2024**, *12*, 1369. [CrossRef]
27. Song, X.; Shi, Y.; Li, G.; Yang, R.; Wang, G.; Zheng, R.; Li, J.; Lyu, Z. Numerical Simulation of Heat Extraction Performance in Enhanced Geothermal System with Multilateral Wells. *Appl. Energy* **2018**, *218*, 325–337. [CrossRef]
28. Ma, W.; Chen, Y.; Wang, Y.; Yang, C.; Yang, C.; Xiao, C.; Liu, G. Multi-Parameter Design and Optimization of Enhanced Geothermal System Based on Unit Effective Permeable Area. *Appl. Therm. Eng.* **2023**, *225*, 120184. [CrossRef]
29. Meng, N.; Gao, X.; Wang, Z.; Li, T. Numerical Investigation and Optimization on Dynamic Power Generation Performance of Enhanced Geothermal System. *Energy* **2024**, *288*, 129901. [CrossRef]
30. Yaghoubi, A.; Hickson, C.J.; Leonenko, Y.; Dusseault, M.B. Probabilistic Assessment of Induced Seismicity at the Alberta No. 1 Geothermal Project Site. *Can. J. Earth Sci.* **2023**, *60*, 294–306. [CrossRef]
31. Chen, Z.; Grasby, S.E.; Liu, X. *Fracture System Analyses of the Mount Meager Area*; Geological Survey of Canada: Ottawa, ON, Canda, 2021.
32. Chen, Z.; Grasby, S.; Deblonde, C.; Liu, X. *AI-Enabled Remote Sensing Data Interpretation for Geothermal Resource Evaluation as Applied to the Mount Meager Geothermal Prospective Area*; Geological Survey of Canada: Ottawa, ON, Canda, 2022.
33. Chai, Y.; Chen, Z.; Yin, S. A Preliminary Analysis of In-Situ Stress at Mount Meager by Displacement Discontinuity Method with Topography and Tectonics Considered. *Energies* **2023**, *16*, 1397. [CrossRef]
34. Huang, W.; Cao, W.; Guo, J.; Jiang, F. An Analytical Method to Determine the Fluid-Rock Heat Transfer Rate in Two-Equation Thermal Model for EGS Heat Reservoir. *Int. J. Heat Mass Transf.* **2017**, *113*, 1281–1290. [CrossRef]
35. Teng, B.; Li, H.; Yu, H. A Novel Analytical Fracture-Permeability Model Dependent on Both Fracture Width and Proppant-Pack Properties. *SPE J.* **2020**, *25*, 3031–3050. [CrossRef]
36. Aliyu, M.D.; Chen, H.-P. Sensitivity Analysis of Deep Geothermal Reservoir: Effect of Reservoir Parameters on Production Temperature. *Energy* **2017**, *129*, 101–113. [CrossRef]
37. Bedre, M.G.; Anderson, B.J. Sensitivity Analysis of Low-Temperature Geothermal Reservoirs: Effect of Reservoir Parameters on the Direct Use of Geothermal Energy. *Trans. Geotherm. Resour. Counc.* **2012**, *36*, 1255–1261.
38. Geoscience BC Mount Meager Geothermal Data Compilation Project. Available online: https://www.geosciencebc.com/projects/2017-006/ (accessed on 28 November 2023).
39. Bodvarsson, G. On the Temperature of Water Flowing Through Fractures. *J. Geophys. Res.* **1969**, *74*, 1987–1992. [CrossRef]
40. Barends, F. Complete Solution for Transient Heat Transport in Porous Media, Following Lauwerier. *Proc. SPE Annu. Tech. Conf. Exhib.* **2010**, *4*. [CrossRef]
41. Voneiff, G.W.; Holditch, S.A. Economic Assessment of Applying Advances in Fracturing Technology. *J. Pet. Technol.* **1994**, *46*, 51–57. [CrossRef]
42. Gkousis, S.; Welkenhuysen, K.; Harcouët-Menou, V.; Pogacnik, J.; Laenen, B.; Compernolle, T. Integrated Geo-Techno-Economic and Real Options Analysis of the Decision to Invest in a Medium Enthalpy Deep Geothermal Heating Plant. A Case Study in Northern Belgium. *Energy Econ.* **2024**, *134*, 107611. [CrossRef]

Disclaimer/Publisher's Note: The statements, opinions and data contained in all publications are solely those of the individual author(s) and contributor(s) and not of MDPI and/or the editor(s). MDPI and/or the editor(s) disclaim responsibility for any injury to people or property resulting from any ideas, methods, instructions or products referred to in the content.